

Subdivision of Uniform Powell-Sabin Splines

Joris Windmolders, Paul Dierckx

Report TW 270, November 1997



Katholieke Universiteit Leuven
Department of Computer Science
Celestijnenlaan 200A – B-3001 Heverlee (Belgium)

Subdivision of Uniform Powell-Sabin Splines

Joris Windmolders, Paul Dierckx

Report TW 270, November 1997

Department of Computer Science, K.U.Leuven

Abstract

We present a subdivision scheme for Powell-Sabin splines on uniform triangulations. As an application we show how to generate efficiently a three-direction wireframe of curves for a given PS-spline surface.

Keywords : Powell-Sabin splines, subdivision, wireframe of curves, normalized B -splines, control points, Bézier net

1 Introduction

Geometric modelling of complex shapes heavily relies on the use of powerful mathematical representations of surfaces. See e.g. Farin (1997), Hoschek and Lasser (1993). Some desired properties of such representations

$$p(u, v) = \sum_{i=1}^N C_i \phi_i(u, v), \quad (u, v) \in \Omega \subset \mathbb{R}^2, \quad C_i \in \mathbb{R}^3 \quad (1)$$

are, for instance,

- being invariant under affine domain transformations;
- the fact that control points can be associated with it, giving us insight in the shape of the surface;
- that it should be possible to make predictable local changes.

In mathematical terms, these properties can be realised by imposing some conditions on the basis functions:

$$\phi_i(u, v) \geq 0, \quad i = 1, \dots, N \quad (2)$$

$$\sum_{i=1}^N \phi_i(u, v) \equiv 1 \quad (3)$$

$$\phi_i(u, v) \text{ has local support, } i = 1, \dots, N \quad (4)$$

Moreover, in order to generate sufficiently smooth surfaces, continuity conditions on the basis functions can be imposed.

Widely used now is the normalised B-spline representation of tensor product splines. Yet, it is restricted to rectangular domains Ω . Farin (1986) studied the Bernstein-Bézier representation of piecewise polynomials on arbitrary conforming triangulations of polygonal domains. Though this approach solves the problem of restrictions on the domain shape, and even if it carries some nice resemblances with the Bernstein-Bézier representation of curves with it, the vouch for smoothness between patches implies nontrivial relations between their coefficients to be kept up, a shortcoming which B-spline representations don't suffer from. Shi et al. (1986) considered a B-spline representation for Powell-Sabin splines but their construction method has some serious drawbacks from the numerical point of view (see Dierckx et al., 1992).

In a recent paper, Dierckx (1997) therefore enunciates an improved algorithm for the construction of a normalised B-spline basis for Powell-Sabin splines. Not only does it preserve C^1 -continuity inherently, it adapts to the kind of triangulation it is constructed upon as well, guaranteeing aforesaid numerical problems to become a matter of history. We will use this representation and its geometrical interpretation here in order to handle the subdivision problem of Powell-Sabin splines on uniform triangulations. We will concentrate on (non-parametric) surfaces $z = s(x, y)$. An extension to parametric surfaces (1) is straightforward.

Section 2 introduces some general items about polynomials on triangulations and recalls the definition of the space of Powell-Sabin splines. It covers the relevant aspects of the construction of a normalised B-spline basis as well. Section 3 shows how the problem of subdivision can be handled on uniform triangulations, and how the coefficients in (1) after refinement can be calculated from the representation on the coarser triangulation. As an application, section 4 covers an algorithm to generate a three-direction wireframe model of a PS-spline surface on a uniform triangulation.

2 Powell-Sabin splines

2.1 Polynomials on the triangle

Consider a non-degenerated triangle $\rho(V_1, V_2, V_3)$ with its vertices having Cartesian coordinates $V_i(x_i, y_i)$, $i = 1, 2, 3$. This triangle will be referred to as the *domain triangle*. The barycentric coordinates (τ_1, τ_2, τ_3) of a point $P(x, y) \in \mathbb{R}^2$ with respect to ρ are the unique solution to the system

$$\begin{bmatrix} x_1 & x_2 & x_3 \\ y_1 & y_2 & y_3 \\ 1 & 1 & 1 \end{bmatrix} \begin{bmatrix} \tau_1 \\ \tau_2 \\ \tau_3 \end{bmatrix} = \begin{bmatrix} x \\ y \\ 1 \end{bmatrix} \quad (5)$$

Letting Π_2 denote the linear space of bivariate polynomials of degree ≤ 2 , each polynomial $P_2(x, y) \in \Pi_2$ on ρ has a unique representation

$$P_2(x, y) = \sum_{|\lambda|=2} b_\lambda B_\lambda^2(\tau), \quad \tau \in \rho \quad (6)$$

with $\lambda = (i, j, k)$, $i, j, k \geq 0$ a multi-index of length $|\lambda| = i + j + k = 2$ and $B_\lambda^2(\tau)$ the Bernstein-Bézier polynomials of degree 2:

$$B_\lambda^2(\tau) = \frac{2!}{i!j!k!} \tau_1^i \tau_2^j \tau_3^k, \quad |\lambda| = 2 \quad (7)$$

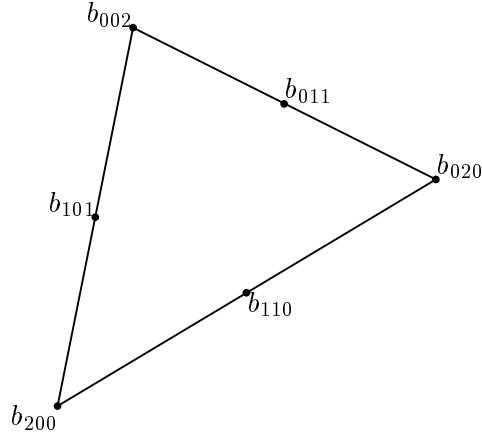


Figure 1: Domain triangle

This Bernstein-Bézier representation of polynomials on the triangle can be reflected schematically by associating each ordinate b_{ijk} with the point $(\frac{i}{2}, \frac{j}{2}, \frac{k}{2})$ in the domain triangle, as in figure 1. We will call these the Bézier triangle points. The Bézier control points are defined as $(\frac{i}{2}, \frac{j}{2}, b_\lambda)$. Their piecewise linear interpolant mimics the form of the polynomial surface $z = P_2(x, y)$. Bernstein-Bézier polynomial topics on triangulations are covered in (Farin, 1986).

2.2 The linear space $S_2^1(\Delta^*)$

Consider a simply connected subset $\Omega \subset \mathbb{R}^2$ with polygonal boundary $\delta\Omega$. Suppose we have a conforming triangulation of Ω , being constituted of triangles ρ_j , $j = 1, \dots, t$, and having vertices V_i with Cartesian coordinates (x_i, y_i) , $i = 1, \dots, n$. The Powell-Sabin refinement of Δ , being denoted as Δ^* , can now be constructed as follows (see figure 2):

1. Find an interior point $Z_j \in \rho_j$, $j = 1, \dots, t$, so that if two triangles ρ_j and ρ_l have a common edge $V_i V_k$, the line joining Z_j and Z_l intersects $V_i V_k$ at a point $Q_{j,l}$ between its vertices. Possible choices for Z_j are the barycenter and the center of the inscribed circle. Whilst the first choice is simple, the second one guarantees the existence of $Q_{j,l}$.
2. Join Z_j to the vertices of ρ_j , $j = 1, \dots, t$.
3. For each edge of ρ_j , $j = 1, \dots, t$:

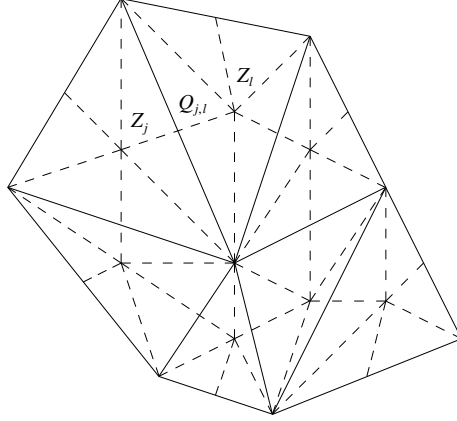


Figure 2: A PS-refinement Δ^*

- which belongs to the boundary $\delta\Omega$, join Z_j to any point on this edge, for instance the midpoint.
- which is common to a triangle ρ_l , join Z_j to $Q_{j,l}$.

Now we consider the space of piecewise quadratic polynomials with C^1 continuity on Ω , the Powell-Sabin splines. It is denoted by $S_2^1(\Delta^*)$. Each of the $6t$ triangles resulting from the PS-refinement thus becomes the domain triangle of a quadratic Bernstein-Bézier polynomial. Powell and Sabin (1977) considered the following interpolation problem:

$$s(V_i) = f_i, \quad \frac{\partial s}{\partial x}(V_i) = f_{xi}, \quad \frac{\partial s}{\partial y}(V_i) = f_{yi}, \quad i = 1, \dots, n \quad (8)$$

and showed a solution $s(x, y)$ always to exist and be unique in $S_2^1(\Delta^*)$. Hence, the dimension of the space $S_2^1(\Delta^*)$ equals $3n$.

2.3 A normalised B-spline representation for PS-splines

This section briefly discusses some important results taken from Dierckx (1997). At first, we need some definitions.

Definition 2.1 *The molecule M_j of vertex V_j consists of the union of all triangles $\rho_i \in \Delta$ having V_j as one of its vertices.*

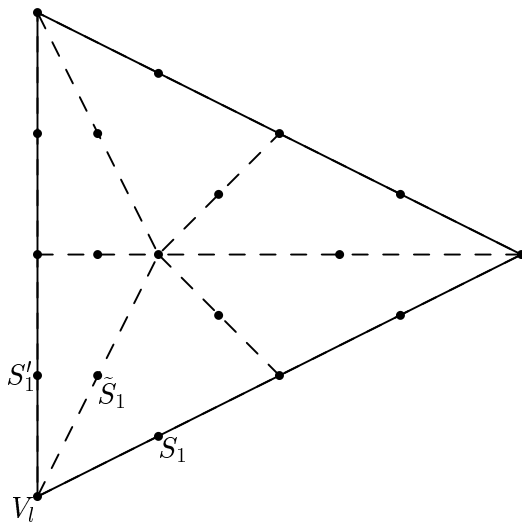


Figure 3: Powell-Sabin points

Definition 2.2 *The molecule number m_j of vertex V_j equals the number of triangles $\rho_i \in \Delta$ in M_j .*

Definition 2.3 *Let the triangles in molecule M_l be numbered $\rho_1, \dots, \rho_{m_l}$ in counterclockwise direction. Consider triangle ρ_1 , see figure 3. The Bézier triangle points have been marked. Note the particular points $V_l, S_1, \tilde{S}_1, S'_1$. We define the Powell-Sabin triangle points of V_l as the points $V_l, S_1, \tilde{S}_1, \dots, S_{m_l}, \tilde{S}_{m_l}, S'_{m_l}$.*

We are looking for a B-spline representation

$$s(x, y) = \sum_{i=1}^n \sum_{j=1}^3 c_{i,j} B_i^j(x, y) \quad , \quad (x, y) \in \Omega \quad (9)$$

in which the basis functions have local support. Such a basis can be computed as follows: find 3 linearly independent sets $(\alpha_{l,j}, \beta_{l,j}, \gamma_{l,j})$, $j = 1, 2, 3$ for each vertex V_l . Solve the interpolation problem (8) with $(f_i, f_{xi}, f_{yi}) = (0, 0, 0)$, except for $i = l$, $(f_l, f_{xl}, f_{yl}) = (\alpha_{l,j}, \beta_{l,j}, \gamma_{l,j})$ as to obtain $B_l^j(x, y)$.

The sets $(\alpha_{l,j}, \beta_{l,j}, \gamma_{l,j})$, $j = 1, 2, 3$ are determined with the objective of also satisfying (2)-(3) in mind. There is an interesting geometric interpretation of this problem. It is shown that a one-to-one correspondence exists

between the sets $(\alpha_{l,j}, \beta_{l,j}, \gamma_{l,j})$, $j = 1, 2, 3$ and the vertices $Q_{l,j}(X_{l,j}, Y_{l,j})$ of a triangle in the domain plane:

$$\begin{bmatrix} \alpha_{l,1} & \alpha_{l,2} & \alpha_{l,3} \\ \beta_{l,1} & \beta_{l,2} & \beta_{l,3} \\ \gamma_{l,1} & \gamma_{l,2} & \gamma_{l,3} \end{bmatrix} \begin{bmatrix} X_{l,1} & Y_{l,1} & 1 \\ X_{l,2} & Y_{l,2} & 1 \\ X_{l,3} & Y_{l,3} & 1 \end{bmatrix} = \begin{bmatrix} x_l & y_l & 1 \\ 1 & 0 & 0 \\ 0 & 1 & 0 \end{bmatrix} \quad (10)$$

Moreover, the conditions (2)-(3) will be satisfied if and only if the triangle $t_l(Q_{l,1}, Q_{l,2}, Q_{l,3})$, called PS-triangle, contains the PS-triangle points of V_l . It appears that the coordinates $X_{l,j}$, $Y_{l,j}$ are nothing but the coefficients of the representation of the polynomials $P_x(x, y) = x$ and $P_y(x, y) = y$ as PS-splines with respect to the considered basis, i.e.

$$P_x(x, y) = \sum_{i=1}^n \sum_{j=1}^3 X_{i,j} B_i^j(x, y) \quad (11)$$

$$P_y(x, y) = \sum_{i=1}^n \sum_{j=1}^3 Y_{i,j} B_i^j(x, y) \quad (12)$$

Another useful consequence is the notion of control triangles. Hereto, we define the PS-control points as

$$C_{l,j}(X_{l,j}, Y_{l,j}, c_{l,j}) \quad (13)$$

For fixed l , they constitute a triangle $T_l(C_{l,1}, C_{l,2}, C_{l,3})$ that is tangent to the surface at $(V_l, s(V_l))$.

With these geometric considerations in mind, we can now develop a strategy to determine $(\alpha_{l,j}, \beta_{l,j}, \gamma_{l,j})$.

- In order for the control triangle to have its control points close to the surface, the triangle t_l of the smallest area that contains the PS-triangle points of V_l can be determined. Computationally, this problem can be reduced to the solution of a quadratic programming problem. We will refer to the corresponding t_l as the *optimal triangle*. This approach will be taken in section 3.1. Examples are given in figure 4.
- It may be worthwhile to premise a valid shape for t_l from which we know in advance that it contains the PS-triangle points, and which is easy to calculate. This approach is taken in section 3.2.

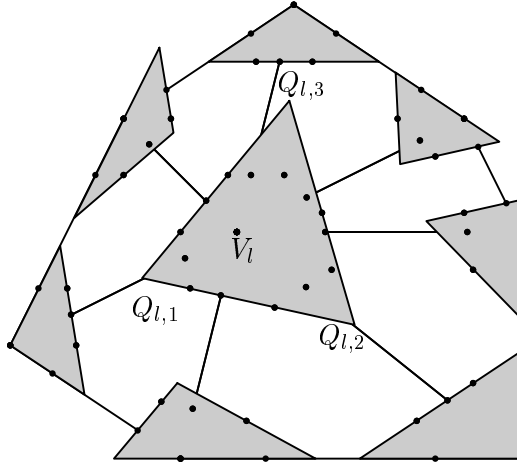


Figure 4: Optimal triangles

Finally, the Bézier control points can be found as convex barycentric combinations of the PS-control points.

3 Subdivision of uniform Powell-Sabin splines

3.1 Equilateral Triangles

In the sequel, we consider a domain Ω being constituted of equilateral triangles. The barycenter of each triangle now coincides with the center of the inscribed circle, and during the PS-refinement procedure we will choose this as the internal point Z_j , $j = 1, \dots, t$. We propose a solution to the subdivision problem: given a PS-spline on Ω , with uniform triangulation Δ , find the representation of the same spline on a uniform refinement Δ' of Δ . Hereto, we add some vertices and split up each triangle as follows (see figure 5):

1. For each edge $V_k V_l$, add the vertex $V'_{kl} = \frac{1}{2}(V_k + V_l)$.
2. Replace each triangle $\rho_{i,j,k}(V_i, V_j, V_k)$ by the 4 smaller triangles it covers, i.e. $\rho'_{i,ij,ik}(V_i, V_{ij}, V_{ik})$, $\rho'_{j,jk,ij}(V_j, V_{jk}, V_{ij})$, $\rho'_{k,ik,jk}(V_k, V_{ik}, V_{jk})$ as well as $\rho'_{ij,jk,ik}(V_{ij}, V_{jk}, V_{ik})$.

From the construction, it follows that

- the lines of C^2 -discontinuity at successive refinements coincide;

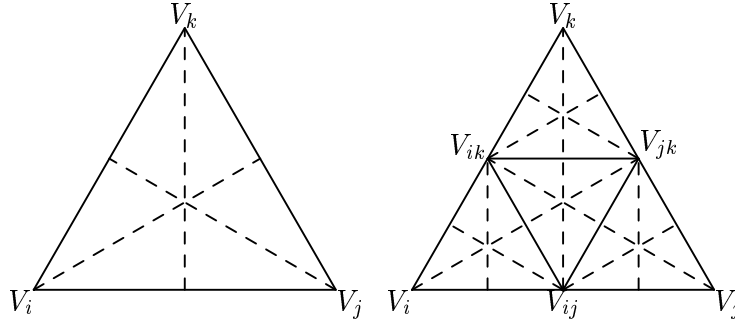


Figure 5: Uniform refinement

- the number of vertices increases as $n' = 2n + t - 1$;
- the number of triangles increases as $t' = 4t$.

Now we return to the construction of a normalised B-spline basis corresponding to the triangulation Δ . The high degree of symmetry invites us to work more efficiently than solving a quadratic programming problem for each vertex. Indeed, in a uniform triangulation only a limited number of molecule configurations appear. Figure 6 shows a uniform domain with molecules having $m_l = 1, 2, 3, 6$. Any two molecules with the same molecule number are isomorphic, so we consider but different molecule numbers.

A molecule with a particular m_l has a certain configuration of the PS-triangle points belonging to V_l that determine the optimal triangle t_l . Hence, the shape of the optimal triangle corresponding to each m_l can be calculated once and for all. Any molecule in a possibly coarser or finer triangulation

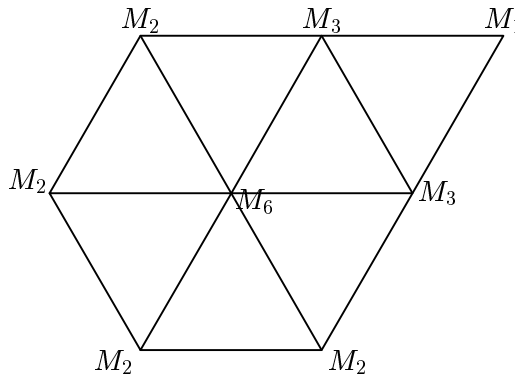


Figure 6: Possible molecules

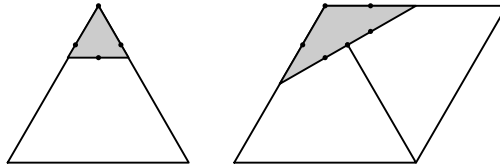


Figure 7: Molecule numbers one and two.

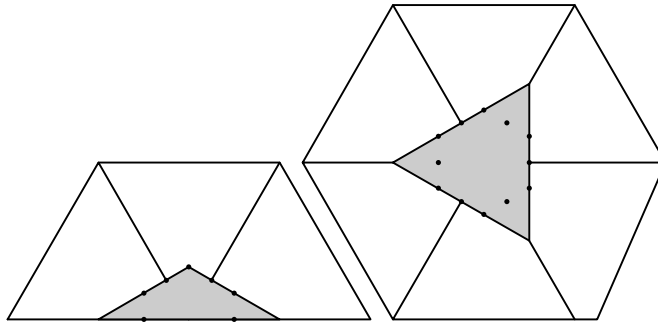


Figure 8: Molecule numbers three and six.

with the same m_l -value will have an isomorphic optimal triangle; there is no need to solve quadratic programming programs anymore. Figures 7-8 show the optimal triangles for different molecule numbers; figure 9 shows an example of a triangulation with its optimal triangles. Finally it can be noted that the optimal triangle corresponding to $m_l = 6$ is equilateral itself and has its vertices halfway the edges of Δ . V_l is at the barycenter of t_l . Moreover, two optimal solutions exist: the one given in figure 8 and the one given in the middle of figure 9.

3.2 A fixed form for the PS-triangles

From figure 9, it follows that the area of the optimal triangle increases with m_l . Denote with $t(M_{m_l})$ the optimal triangle corresponding to a certain molecule having $m_l \in \{1, 2, 3, 6\}$, then it is clear that at a certain vertex, the optimal triangle $t(M_k)$ can be replaced by any $t(M_j)$, $j > k$. More particularly, any $t(M_k)$ can be replaced by $t(M_6)$. Fixing the form of the PS-triangles to $t(M_6)$ will be shown to lead to very efficient calculations in the subdivision problem. Moreover, it leaves the possibility to join certain domains at a border, without having to recalculate the global representation

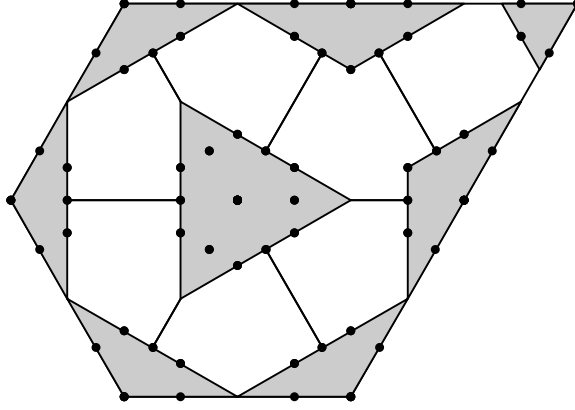


Figure 9: Triangulation and optimal triangles.

of the surface.

Two important consequences are considered:

1. The Bézier control points can be determined with particularly simple convex barycentric combinations of the PS-control points $C_{l,j}$.
2. The PS-control points after refinement can be written as particularly simple barycentric convex combinations of the ones before refinement.

We will use the following notation:

$$k_3 = \begin{cases} 3, & k = 3n, \quad n \in \mathbb{Z} \\ k \bmod 3, & \text{else} \end{cases} \quad (14)$$

As for the first property, we simply have to apply a result from Dierckx (1997) which yields, in accordance with figure 11:

$$\begin{cases} s_l &= \frac{1}{3}(C_{l1} + C_{l2} + C_{l3}) \\ u_l &= \frac{1}{2}(C_{l(l+1)_3} + C_{l(l+2)_3}) \\ v_l &= \frac{2}{3}C_{l(l+2)_3} + \frac{1}{6}(C_{ll} + C_{l(l+1)_3}) \\ w_l &= \frac{1}{3}C_{l(l+1)_3} + \frac{2}{3}C_{l(l+2)_3} \end{cases} \quad (15)$$

$$\begin{cases} r_l &= \frac{1}{2}(v_{(l+2)_3} + u_{(l+1)_3}) \\ \theta_l &= \frac{1}{2}(w_{(l+1)_3} + w_{(l+2)_3}) \end{cases} \quad (16)$$

where $l=1,2,3$, and

$$\omega = \frac{1}{3}(\theta_1 + \theta_2 + \theta_3) \quad (17)$$

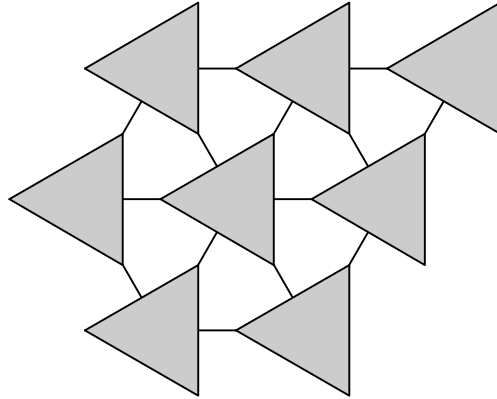


Figure 10: A fixed form for the triangles $t_l(Q_{l,1}, Q_{l,2}, Q_{l,3})$.

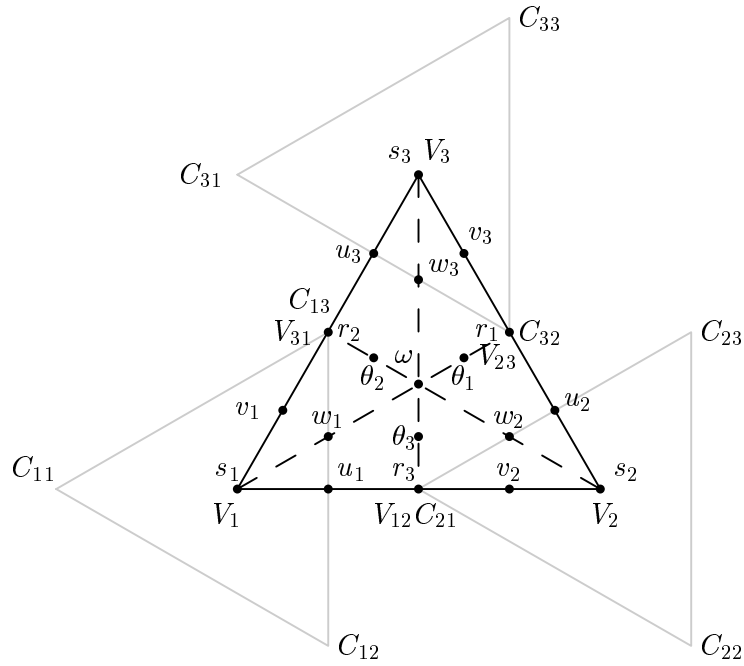


Figure 11: Bézier points and control triangles.

To prove the second property, we distinguish between *old vertices*, those are the vertices that appear in the coarser triangulation, and *new vertices*, those are vertices that appear in the refined triangulation but not in the

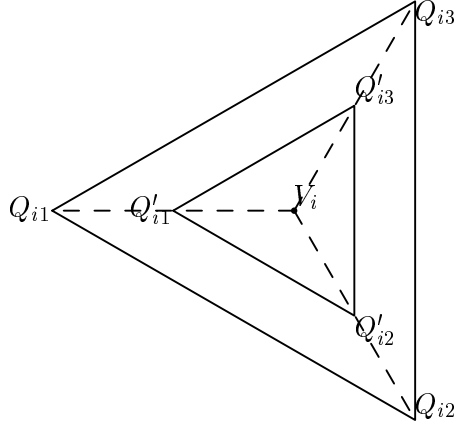


Figure 12: The new PS-triangle in V_i .

coarse one. PS-triangles from the coarser triangulation will be denoted by $t_i(Q_{i,1}, Q_{i,2}, Q_{i,3})$ and the ones arising in the refinement will be denoted by $t'_i(Q'_{i,1}, Q'_{i,2}, Q'_{i,3})$. If we write $(Q'_{i,1}, Q'_{i,2}, Q'_{i,3})$ as convex barycentric combinations of $(Q_{i,1}, Q_{i,2}, Q_{i,3})$, from the physical interpretation of the control net it then follows that the same combinations are valid for the PS-control points $C'_{i,j}$ and $C_{i,j}$, $j = 1, 2, 3$.

Old vertices. It is clear that the old and new control triangle in a certain vertex are coplanar. Looking at the PS-triangle (see figure 12), it follows from the geometry and the properties mentioned in section 3.1:

$$Q'_{i3} = \frac{1}{2} \left(\frac{1}{3}(Q_{i1} + Q_{i2} + Q_{i3}) + Q_{i3} \right) \quad (18)$$

The same expression applies to the B-spline control points, and similar reasoning on Q_{i1} and Q_{i2} finally delivers

$$C'_{il} = \frac{2}{3}C_{il} + \frac{1}{6}(C_{i(l+1)3} + C_{i(l+2)3}), \quad l = 1, 2, 3 \quad (19)$$

These are clearly convex barycentric combinations.

New vertices $V'_i = V_{k,l}$. Consider a new vertex $V_{3,1}$ halfway between V_3 and V_1 (see figure 13), common edge of the triangles $\rho(V_1, V_2, V_3)$ and $\rho(V_3, V_4, V_1)$. We denote the new PS-triangle by $t'_{31}(Q_{311}, Q_{312}, Q_{313})$. From

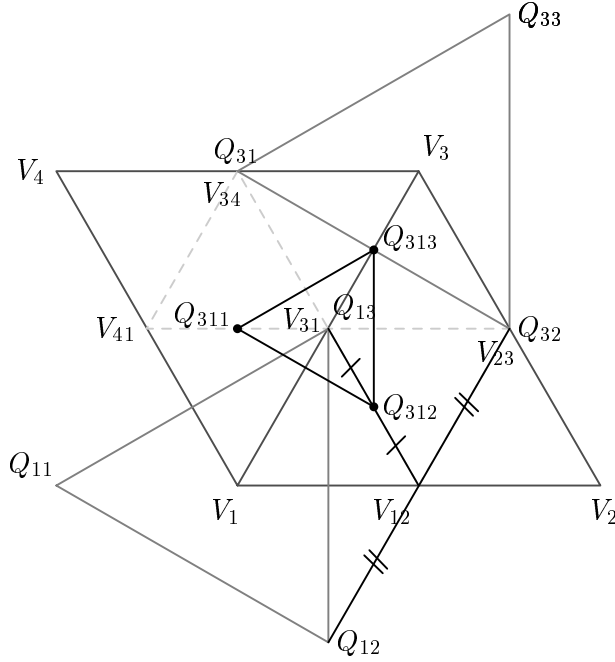


Figure 13: Triangle $t'(Q_{311}, Q_{312}, Q_{313})$.

the geometry, it follows:

$$Q_{312} = \frac{1}{2} \left(\frac{1}{2} (Q_{12} + Q_{32}) + Q_{13} \right) \quad (20)$$

Similar reasoning on $Q_{3,1,1}$ and $Q_{3,1,3}$, applied to the B-spline control points leads to:

$$\begin{cases} C_{311} = \frac{1}{2} C_{13} + \frac{1}{4} (C_{11} + C_{31}) \\ C_{312} = \frac{1}{2} C_{13} + \frac{1}{4} (C_{12} + C_{32}) \\ C_{313} = \frac{1}{2} (C_{31} + C_{32}) \end{cases} \quad (21)$$

The control triangles on the edges $V_1 - V_2$ and $V_2 - V_3$ (see figure 14) are found analogously. Now we come to a general statement: a new control triangle arises on an edge $V_i - V_j$, $i \neq j$, $i, j \in \{1, 2, 3\}$. The vertices are ordered as follows:

- West-East (e.g. $V_1 - V_2$ and $V_4 - V_3$)
- Southeast-Northwest (e.g. $V_2 - V_3$ and $V_1 - V_4$)
- Northeast-Southwest (e.g. $V_3 - V_1$).

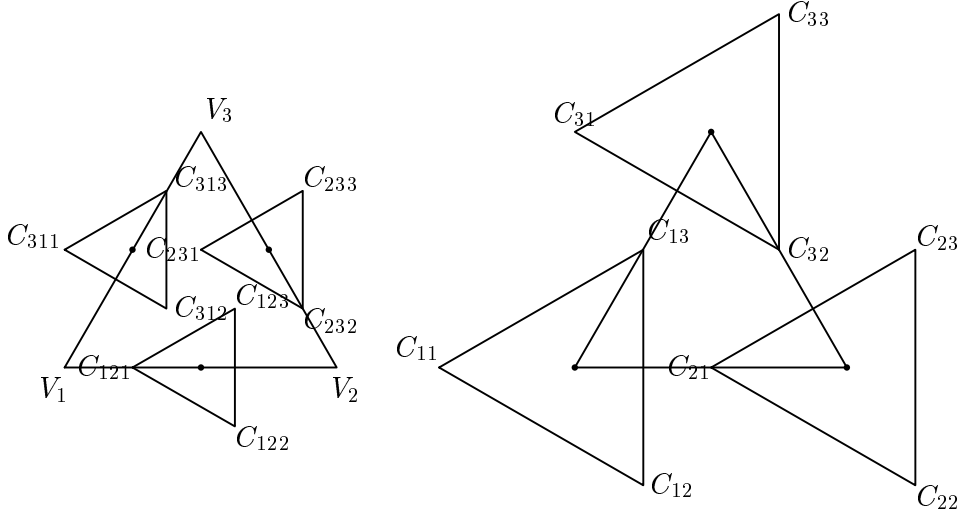


Figure 14: Left side: new control triangles; right side: old control triangles

It follows:

$$\begin{cases} C_{iji} &= \frac{1}{2}(C_{i(i+1)_3} + C_{i(i+2)_3}) \\ C_{ij(i+1)_3} &= \frac{1}{2}C_{ji} + \frac{1}{4}(C_{j(i+1)_3} + C_{i(i+1)_3}) \\ C_{ij(i+2)_3} &= \frac{1}{2}C_{ji} + \frac{1}{4}(C_{j(i+2)_3} + C_{i(i+2)_3}) \end{cases} \quad (22)$$

These are all convex barycentric combinations. Figure 15 shows the refinement with uniform PS–triangles of the triangulation from figure 10.

3.3 Parametric PS–splines

We briefly touch the straightforward generalisation to parametric surfaces. A collection of points

$$\begin{cases} x = s_x(u, v) = \sum_{i=1}^n \sum_{j=1}^3 c_{i,j}^x B_i^j(u, v) \\ y = s_y(u, v) = \sum_{i=1}^n \sum_{j=1}^3 c_{i,j}^y B_i^j(u, v) \\ z = s_z(u, v) = \sum_{i=1}^n \sum_{j=1}^3 c_{i,j}^z B_i^j(u, v) \end{cases} \quad (23)$$

where $(u, v) \in \Omega$, $s_l \in S_2^1(\Delta^*)$, $l = x, y, z$ defines a parametric PS–spline surface in its normalised B–spline representation. Each component is a piecewise quadratic polynomial with C^1 -continuity on Δ . Given such a triangulation Δ , the basis can be constructed as in section 2. Subdivision on uniform triangulations can be applied to each component. If we define

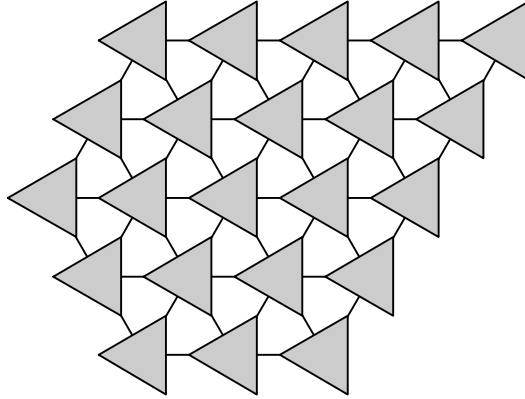


Figure 15: Uniform refinement

the B-spline control points

$$C_{l,j}(c_{l,j}^x, c_{l,j}^y, c_{l,j}^z) \quad j = 1, 2, 3 \quad (24)$$

the triangle $T_l(C_{l,1}, C_{l,2}, C_{l,3})$ can easily be proven to be tangent to the parametric surface at $s(V_l) = (s_x(V_l), s_y(V_l), s_z(V_l))$. For $s_x(x, y) = x$ and $s_y(x, y) = y$, (24) reduces to (13).

4 Construction of a three-direction wireframe

It is customary to visualise bicubic B-spline surfaces on rectangular domains with two-direction wireframe models. As an application of formulae (19),(22) we show how a three-direction wireframe model of the PS-spline surface can be efficiently constructed.

4.1 A matrix structure

From the uniform triangulation Δ we can deduce a naturally associated matrix structure containing control triangle data.

step 1. Extend the triangulation with the smallest number of triangles so that a parallelogram with its baseline shifted to the right arises, and denote it with $\tilde{\Delta}$. Figure 16 shows the extension of the known domain with dashed lines. New vertices have been introduced, so we have to distinguish between

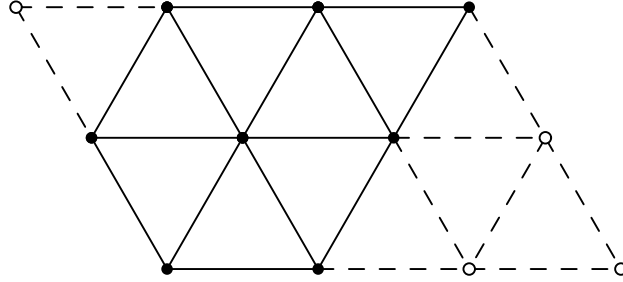


Figure 16: An extended triangulation

- real vertices (black dots)
- pseudo-vertices (circles)

step 2. Think of this triangulation as a movable grid, and recast it into a rectangle (see figure 17). Call this the *associated grid* R , with r horizontal lines and c vertical lines.

step 3. • With each vertex V_l of the grid, corresponding to a real vertex of $\tilde{\Delta}$, we associate a 3×3 matrix B , defined as

$$\begin{bmatrix} C_{l,1} \\ C_{l,2} \\ C_{l,3} \end{bmatrix} \quad (25)$$

referring to (13) for a surface $z = s(x, y)$, or (24) in the parametric case.

- With each vertex of the grid, corresponding to a pseudo-vertex of $\tilde{\Delta}$, we associate a 3×3 zero matrix B .

step 4. All those tiny matrices, located at the position of the corresponding grid point, constitute a block matrix structure M with r blockrows and c blockcolumns (see figure 18). Call M the *associated matrix structure* of the grid R , and denote the block matrices by $B_{k,l}$, or, more generally, the *B-matrices*, and let the corresponding vertex be written as $V_{k,l} \in \tilde{\Delta}$, $k = 1, \dots, r$, $l = 1, \dots, c$.

From the construction it follows:

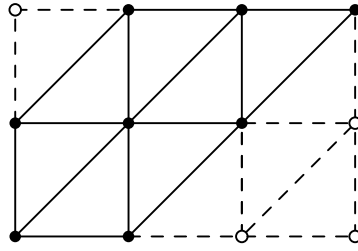


Figure 17: Associated grid R .

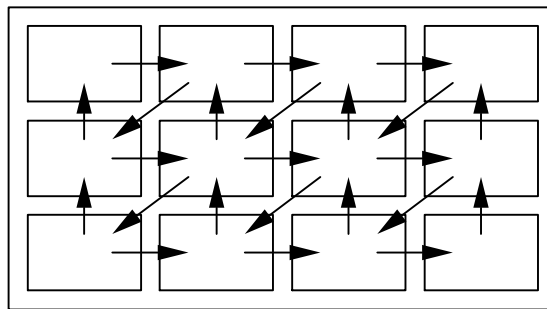


Figure 18: Associated matrix structure M .

Property 4.1 *West-east connections.*

For $i = 1, \dots, r$
 For $j = 1, \dots, c - 1$,
 vertex $V_{i,j}$ is connected with vertex $V_{i,j+1}$

These are the *west-east connections* from section 3.2, painted as horizontal arrows in figure 18.

Property 4.2 *Southeast-Northwest connections.*

For $i = 2, \dots, r$
 For $j = 1, \dots, c$,
 Vertex $V_{i,j}$ is connected with vertex $V_{i-1,j}$

These are the *Southeast-Northwest connections* from section 3.2, painted as vertical arrows in figure 18.

Property 4.3 *Northeast-Southwest connections.*

For $i = 1, \dots, r - 1$
 For $j = 2, \dots, c$,
 Vertex $V_{i,j}$ is connected with vertex $V_{i+1,j-1}$

These are the *Northeast-Southwest connections* from section 3.2, painted as oblique arrows in figure 18.

Next, the triangulation is subdivided. Using local matrix operations on M , a new structure M' should be deduced, which is the matrix structure associated with the extended refined triangulation $\tilde{\Delta}'$. Thinking of the B -matrices as control triangles and the arrows as edges, it is clear that the subdivision process causes new B' -matrices to appear everywhere new control triangles arise:

- at the position of the original B -matrices;
- halfway the arrows.

Figure 19 shows the structure M' ; the B' -matrices corresponding to the arrows have been shaded. The number of rows and columns increase as

$$r' = 2r - 1 \quad c' = 2c - 1. \quad (26)$$

To distinguish the real from the pseudo-vertices, let the first and last position of a real vertex in row i be denoted by $k_{i,1}$ resp. $k_{i,2}$. They evolve like

$$k'_{2i-1,j} = 2k_{i,j} - 1, \quad j = 1, 2 \quad (27)$$

for $i = 1, \dots, r$ and

$$k'_{2i,j} = \frac{1}{2}(k'_{2i-1,j} + k'_{2i+1,j}), \quad j = 1, 2 \quad (28)$$

for $i = 1, \dots, r - 1$.

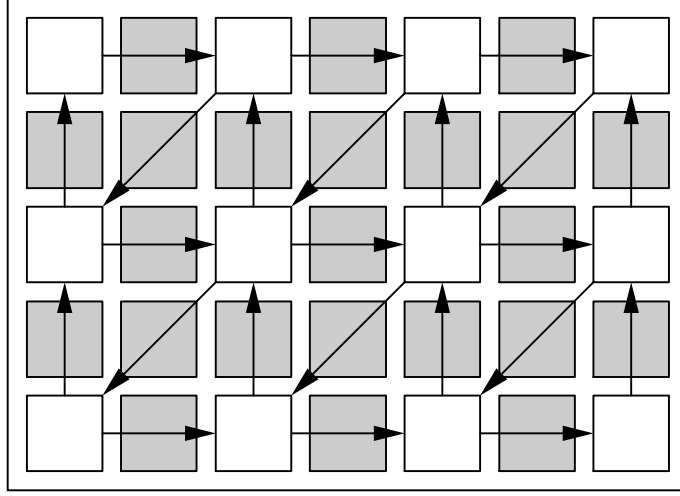


Figure 19: Matrix structure M' .

4.2 Local matrix operations

The local matrix operations allowing to calculate B' from B can be derived from (19) and (22), i.e.

$$B'_{2k-1,2l-1} = B_{k,l} \begin{bmatrix} \frac{2}{3} & \frac{1}{6} & \frac{1}{6} \\ \frac{1}{6} & \frac{2}{3} & \frac{1}{6} \\ \frac{1}{6} & \frac{1}{6} & \frac{2}{3} \end{bmatrix}, \quad k = 1, \dots, r, \quad l = 1, \dots, c$$

$$B'_{2k-1,2l} = B_{k,l} \begin{bmatrix} 0 & 0 & 0 \\ \frac{1}{2} & \frac{1}{4} & 0 \\ \frac{1}{2} & 0 & \frac{1}{4} \end{bmatrix} + B_{k,l+1} \begin{bmatrix} 0 & \frac{1}{2} & \frac{1}{2} \\ 0 & \frac{1}{4} & 0 \\ 0 & 0 & \frac{1}{4} \end{bmatrix} \quad k = 1, \dots, r, \quad l = 1, \dots, c-1$$

$$B'_{2k,2l-1} = B_{k+1,l} \begin{bmatrix} \frac{1}{4} & \frac{1}{2} & 0 \\ 0 & 0 & 0 \\ 0 & \frac{1}{2} & \frac{1}{4} \end{bmatrix} + B_{k,l} \begin{bmatrix} \frac{1}{4} & 0 & 0 \\ \frac{1}{2} & 0 & \frac{1}{2} \\ 0 & 0 & \frac{1}{4} \end{bmatrix} \quad k = 1, \dots, r-1, \quad l = 1, \dots, c$$

$$B'_{2k,2l} = B_{k,l+1} \begin{bmatrix} \frac{1}{4} & 0 & \frac{1}{2} \\ 0 & \frac{1}{4} & \frac{1}{2} \\ 0 & 0 & 0 \end{bmatrix} + B_{k+1,l} \begin{bmatrix} \frac{1}{4} & 0 & 0 \\ 0 & \frac{1}{4} & 0 \\ \frac{1}{2} & \frac{1}{2} & 0 \end{bmatrix} \quad k = 1, \dots, r-1, \quad l = 1, \dots, c-1$$

4.3 Construction of the wireframe

After a few refinement steps, the points on the PS-spline surface are generated as follows:

$$\begin{aligned} &\text{For } i = 1, \dots, r \\ &\quad \text{For } j = 1, \dots, c, \\ &\quad \quad p(i, j) = B_{ij} \left(\frac{1}{3} \ \frac{1}{3} \ \frac{1}{3} \right)^T \end{aligned}$$

The actual data that eventually will be displayed, are obtained by selecting the real vertices from the extended triangulation and joining them, yielding a wireframe. Figures 20–22 show a wireframe at consecutive refinement steps.

Normal vectors It is now possible to calculate the normal vectors n_l at the tangent points as well. Therefore, we simply apply:

$$n_l = (C_{l,2} - C_{l,1}) \times (C_{l,3} - C_{l,1}). \quad (29)$$

5 Concluding Remarks

It is possible to derive equations analogously to (19) and (22) for finer subdivisions. We briefly mention the case in which each triangle ρ_j , $j = 1, \dots, t$ is subdivided into 9 smaller equilateral triangles of equal area. New control triangles in old vertices are found as:

$$C'_{i,l} = \frac{2}{3} \left(\frac{1}{3} C_{i,1} + \frac{1}{3} C_{i,2} + \frac{1}{3} C_{i,3} \right) + \frac{1}{3} C_{i,l}, \quad l = 1, 2, 3. \quad (30)$$

Two new control triangles arise on each edge $V_i V_j$ of Δ :

$$\begin{cases} C'_{iji} &= \frac{1}{3} \left(\frac{2}{3} C_{i(i+1)_3} + \frac{1}{3} \left(\frac{2}{3} C_{jj} + \frac{1}{3} C_{ji} \right) \right) + \frac{1}{3} \left(\frac{2}{3} C_{i(i+2)_3} \right. \\ &\quad \left. + \frac{1}{3} \left(\frac{2}{3} C_{j(j+1)_3} + \frac{1}{3} C_{ji} \right) \right) + \frac{1}{3} C_{ji} \\ C'_{ij(i+1)_3} &= \frac{1}{3} \left(\frac{1}{3} C_{ij} + \frac{2}{3} C_{jj} \right) + \frac{2}{3} \left(\frac{1}{9} C_{jj} + \frac{1}{9} C_{j(j+1)_3} + \frac{7}{9} C_{j(j+2)_3} \right) \\ C'_{ij(i+2)_3} &= \frac{1}{3} \left(\frac{1}{3} C_{i(i+2)_3} + \frac{2}{3} C_{j(j+1)_3} \right) + \frac{2}{3} \left(\frac{1}{9} C_{j(j+1)_3} + \frac{1}{9} C_{jj} + \frac{7}{9} C_{ji} \right) \end{cases} \quad (31)$$

$$\begin{cases} C_{iji}^2 &= \frac{4}{9}C_{ij} + \frac{4}{9}C_{i(j+1)_3} + \frac{1}{9}C_{i(j+2)_3} \\ C_{ij(i+1)_3}^2 &= \frac{1}{3}\left(\frac{2}{3}C_{ij} + \frac{1}{3}C_{jj}\right) + \frac{2}{3}\left(\frac{1}{3}C_{ij} + \frac{1}{3}C_{ji} + \frac{1}{3}C_{i(i+2)_3}\right) \\ C_{ij(i+2)_3} &= \frac{1}{3}\left(\frac{2}{3}C_{i(i+2)_3} + \frac{1}{3}C_{j(j+1)_3}\right) + \frac{2}{3}\left(\frac{1}{3}C_{i(i+2)_3} + \frac{1}{3}C_{ij} + \frac{1}{3}C_{ji}\right) \end{cases} \quad (32)$$

As for the new control triangles in the barycenters of ρ_j , we have to distinguish between $\rho_j \in \Delta$ having its apex upward, i.e.

$$C_l = \frac{2}{3}\left(\frac{2}{3}C_{l(l+2)_3} + \frac{1}{3}C_{l(l+1)_3}\right) + \frac{1}{3}\left(\frac{2}{3}C_{(l+2)_3(l+1)_3} + \frac{1}{3}C_{(l+2)_3l}\right), \quad l = 1, 2, 3 \quad (33)$$

and triangles having its apex downward, i.e.

$$C_l = \frac{2}{3}\left(\frac{2}{3}C_{(l+1)_3l} + \frac{1}{3}C_{(l+1)_3(l+2)_3}\right) + \frac{1}{3}\left(\frac{2}{3}C_{(l+2)_3(l+1)_3} + \frac{1}{3}C_{(l+2)_3l}\right), \quad l = 1, 2, 3 \quad (34)$$

A finer subdivision scheme can be obtained by applying (19) and (22) twice. It is clear that these refinements yield wireframes converging to the surface more rapidly, whereas the formulae are equally simple.

Finally it can be noted that not all three directions of the wireframe have to be drawn; a two-direction wireframe could give us valuable insight in the shape of the surface as well.

References

- [1] Dierckx, P., Van Leemput, S. and Vermeire, T. (1992), Algorithms for surface fitting using Powell–Sabin splines, *IMA Journal of Numerical Analysis* 12, 271–299.
- [2] P. Dierckx (1997), On calculating normalized Powell-Sabin B-splines, *Computer Aided Geometric Design* 20, to appear.
- [3] Farin, G. (1986), Triangular Bernstein–Bézier patches, *Computer Aided Geometric Design* 3, 83–127.
- [4] Farin, G. (1997), *Curves and surfaces for Computer Aided Geometric Design; a practical guide*, 4th edition, Academic Press, Boston.
- [5] Hoschek, J. and Lasser, D.(1993), *Fundamentals of Computer Aided Geometric Design*, AK Peeters, Wellesley MA.

- [6] Powell, M. J. D. and Sabin, M. A. (1977), Piecewise quadratic approximations on triangles, *ACM Transactions on Mathematical Software* 3, 316–325.
- [7] Shi, X., Wang, S., Wang, W. and Wang, R. H. (1986), The C^1 -quadratic spline space on triangulations, Report 86004, Department of Mathematics, Jilin University, Changchun.

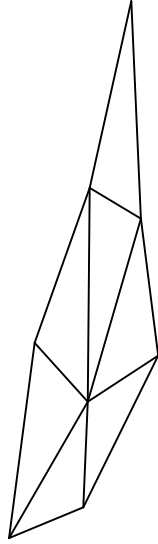


Figure 20: Wireframe without refinement

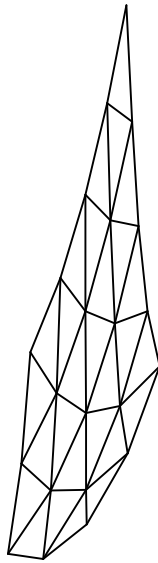


Figure 21: One refinement step

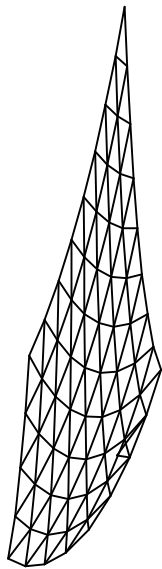


Figure 22: Two refinement steps